

Performance of an M -QAM full-duplex wireless system with a nonlinear amplifier

Zhaojun HE¹, Wanzhi MA¹, Shihai SHAO¹, Fei WU¹,
Chaojin QING² & Youxi TANG^{1*}

¹National Key Laboratory and Technology on Communications, University of Electronic Science and Technology of China, Chengdu 611731, China;

²School of Electrical and Information Engineering, Xihua University, Chengdu 6110039, China

Received October 11, 2015; accepted November 29, 2015; published online March 4, 2016

Abstract The effect of amplifier nonlinearity is analyzed for M -QAM full-duplex communications in additive white Gaussian noise channels. Two classical memoryless nonlinear amplifier models, i.e., a traveling-wave tube amplifier and a solid-state power amplifier, are considered. An analytical expression for the bit error ratio is derived using a characteristic function and numerical integration. Theoretical results show perfect agreement with those obtained by simulation. The analytical results could be used to evaluate the degradation in performance of an M -QAM full-duplex system caused by amplifier nonlinearity, and will be helpful in finding the optimal static operating point of an amplifier.

Keywords full-duplex, amplifier nonlinear distortion, bit error ratio, amplitude error, phase error

Citation He Z J, Ma W Z, Shao S H, et al. Performance of an M -QAM full-duplex wireless system with a nonlinear amplifier. *Sci China Inf Sci*, 2016, 59(10): 102307, doi: 10.1007/s11432-015-5370-2

1 Introduction

The radio spectrum has become one of the scarcest resources with the rapid development of wireless communication technologies [1, 2]. Full-duplex wireless communications can simultaneously transmit and receive signals in the same band. Compared with a traditional half-duplex system, an ideal full-duplex system can obtain double the throughput, which has attracted significant attention recently in academia and industry, and work is now in progress to include full-duplex technology in future 5G mobile standards [3].

However, full-duplex wireless communications suffer from strong self-interference [4], and the key point is how to remove the strong self-interference perfectly (e.g., 100 dB higher than the desired signal) [3]. Three types of self-interference cancellation (SIC) method are considered: antenna cancellation [5–8], analog cancellation [5, 8, 9] and digital cancellation [5–12]. By using a Wi-Fi signal and combining with three cancellation methods [9], a maximum of 100 dB SIC can be achieved.

Usually, there are two cases for the reference signal paths during the analog cancellation stage [13]:

*Corresponding author (email: tangyx@uestc.edu.cn)

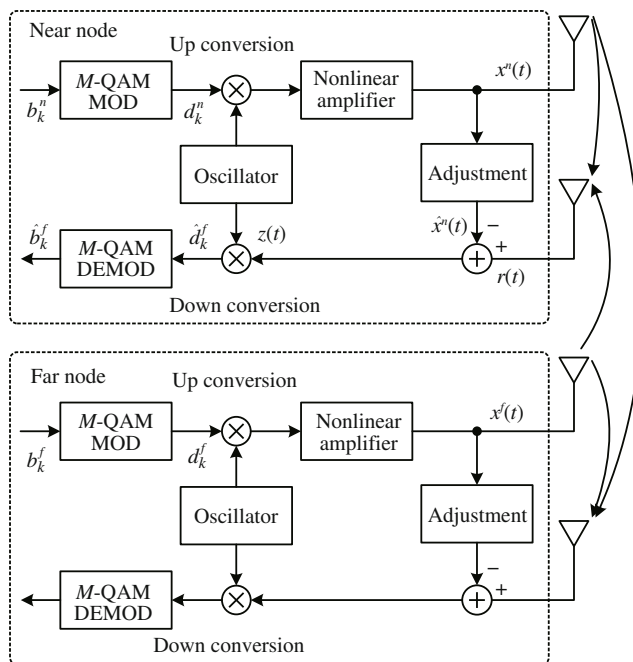


Figure 1 Transceiver block diagrams of an M -QAM full-duplex wireless system.

- Case A describes perhaps the most widely used architecture for taking a reference signal from the output of an amplifier. Groups of attenuators are needed in this approach to make the power of the reference signal match the received signal. Typically, 16 adjustable attenuators and delay lines are used for analog cancellation, and a maximum of 45 dB SIC has been achieved for a 80 MHz bandwidth Wi-Fi signal [14].

- In case B, the reference signal is taken from the input of the amplifier or generated from a third transmission chain, which is known as the Rice University architecture [15]. The problem with this implementation is the nonlinear distortion produced by the amplifier, which is not included in the reference signal.

In this paper, we focus on case B. A digital nonlinear interference cancellation technique is given in [16]. It uses Hammerstein modeling of the nonlinear amplifier and least-squares parameter estimation. The proposed technique enables a higher transmit power to be used compared to existing linear SIC methods. Note that [13,16] do not indicate how much loss of performance was caused by amplifier nonlinearity and how to choose the operating point of an amplifier for a full-duplex wireless communication system.

Thus, we investigate the performance degradation caused by amplifier nonlinearity for an M -QAM full-duplex wireless communication system in an additive white Gaussian noise channel. Considering two classic nonlinear amplifier models, i.e., a traveling-wave tube amplifier (TWTA) and a solid-state power amplifier (SSPA), the bit error ratio (BER) for M -QAM full-duplex wireless communications is derived. From the analyzed results, we can see the performance degradation caused by amplifier nonlinearity compared with an ideal linear amplifier. Using the analysis results in this paper, we can choose the optimal operating point of an amplifier to give a tradeoff between transmission power and performance degradation.

2 System model

Block diagrams for full-duplex wireless communications are shown in Figure 1. The two communication nodes are the far node and the near node, both of which have the same hardware architecture and parameters. For simplicity and without loss of generality, we consider the received signal at the near node, since, due to hardware symmetry, the same analysis applies to the far node [17].

2.1 Transmission system model

The transmitted signal from the far node can be written as

$$x^f(t) = \sqrt{P_f} G \left[\sum_{k=-\infty}^{+\infty} d_k^f h(t - kT) \right] e^{j2\pi f_c t}, \quad (1)$$

where P_f is the transmission power, $G(\cdot)$ is the normalized gain function of the amplifier, d_k^f is the k th M -QAM modulated symbol, T is the symbol period, f_c is the carrier frequency and $h(t)$ is the shaping pulse.

The transmitted signal from the near node can be written as

$$x^n(t) = \sqrt{P_n} G \left[\sum_{k=-\infty}^{+\infty} d_k^n h(t - kT) \right] e^{j(2\pi f_c t + \phi)}, \quad (2)$$

where P_n is the transmission power, d_k^n is the k th M -QAM symbol and ϕ^n is the initial phase of the carrier.

The received signal at the near node antenna is given by

$$r(t) = x^f(t) + x^n(t - \tau) + n(t), \quad (3)$$

where τ is the relative transmission delay of the near signal and $n(t)$ is additive white Gaussian noise with a single-sided power spectrum density of N_0 .

2.2 Nonlinear power amplifier model

The gain for power amplifier distortion is given by [18]

$$G(r) = r \cdot A(|r|) \exp[j\Phi(|r|)], \quad (4)$$

where r is the input signal, $A(|r|)$ is the amplitude distortion of the input amplitude $|r|$, $\Phi(|r|)$ is the phase distortion of the input amplitude $|r|$ and $G(r) = r$ for an ideal linear amplifier. The operating point of an amplifier is usually identified by the output back-off (OBO) [18], which is given by

$$\text{OBO} = 10 \log_{10} \frac{P_{\max}}{P_{\text{out}}} \text{ dB}, \quad (5)$$

where P_{\max} is the maximum output power of the amplifier and P_{out} is the mean power of the current output signal.

In this paper, we consider two classical nonlinear models of an amplifier. For TWTA [18]:

$$A(|r|) = \frac{\alpha_a |r|}{(1 + \beta_a |r|^2)}, \quad \Phi(|r|) = \frac{\alpha_\phi |r|^2}{(1 + \beta_\phi |r|^2)}, \quad (6)$$

where α_a is the small signal gain and $A_s = 1/\sqrt{\beta_a}$ is the amplifier input saturation voltage. The maximum output is $A_0 = \alpha_a A_s/2$. Moreover, the maximum phase displacement is $\phi_\infty = \alpha_\phi/\beta_\phi$. A plausible choice of these parameters is $\alpha_a = 1$, $\beta_a = 0.25$, $\alpha_\phi = \pi/60$ and $\beta_\phi = 0.25$.

For SSPA [18]:

$$A(|r|) = \frac{v \cdot |r|}{[1 + (v \cdot |r|/A_0)^{2p}]^{1/2p}}, \quad \Phi(|r|) = \alpha_\phi \left(\frac{v \cdot |r|}{A_0} \right)^4, \quad (7)$$

where v is the small signal gain, A_0 is the saturating output amplitude, p is a parameter that controls the smoothness of the transition from the linear region to the saturation region and α_ϕ is a phase rotation parameter. Hereafter, we choose $v = 1$, $A_0 = 1$, $\alpha_\phi = \pi/60$ and $p = 2$.

3 Effects of amplifier nonlinearity

3.1 Radio-frequency SIC

At the radio-frequency (RF) front of the near transceiver, the self-interference is first estimated and then removed from the received signal, i.e.,

$$z(t) = r(t) - \hat{x}^n(t), \quad (8)$$

where $\hat{x}^n(t)$ is the estimation of $x^n(t)$, which is given by

$$\hat{x}^n(t) = (1 + \eta)\sqrt{P_n}G \left[\sum_{k=-\infty}^{+\infty} d_k^n h(t - kT - \tau - \Delta\tau) \right] e^{j[2\pi f_c(t - \tau - \Delta\tau) + \phi + \Delta\phi]}, \quad (9)$$

where $\eta \in [-1, 1]$ is the relative estimation error of the amplitude, $\Delta\tau \in [-T/2, T/2]$ is the transmission delay estimation error and $\Delta\phi \in [-180^\circ, 180^\circ]$ is the phase estimation error.

3.2 BER of QAM

The k th decision variable of the near node after matched filtering is

$$\hat{d}_k^f = \frac{1}{\sqrt{P_f}} \int_{-\infty}^{+\infty} z(t) e^{-j2\pi f_c t} * h(kT - t) dt, \quad (10)$$

where $*$ denotes the convolution operation.

Usually, band-limited shaping pulses, e.g., a root raised cosine (RRC), are used in a transceiver. Due to nonlinearity of the amplifier and exhausted inter-symbol interference, the exact final expression of (10) is difficult to obtain. To expound the problem clearly and simply, we choose a special rectangular shaping pulse instead of an RRC pulse, which avoids complicated inter-symbol interference. A comparison of results for rectangular and RRC shaping is given in Section 4. The normalized rectangular shaping pulse is given by

$$h(t) = \begin{cases} \frac{1}{\sqrt{T}}, & 0 \leq t < T, \\ 0, & \text{otherwise.} \end{cases} \quad (11)$$

So, Eqs. (1), (2) and (9) can, respectively, be rewritten as

$$x^f(t) = \sqrt{P_f} \sum_{k=-\infty}^{+\infty} G(d_k^f) h(t - kT) e^{j2\pi f_c t}, \quad (12)$$

$$x^n(t) = \sqrt{P_n} \sum_{k=-\infty}^{+\infty} G(d_k^n) h(t - kT) e^{j(2\pi f_c t + \phi)}, \quad (13)$$

and

$$\hat{x}^n(t) = (1 + \eta)\sqrt{P_n} \sum_{k=-\infty}^{+\infty} G(d_k^n) h(t - kT - \tau - \Delta\tau) e^{j[2\pi f_c(t - \tau - \Delta\tau) + \phi + \Delta\phi]}. \quad (14)$$

By substituting (12)–(14) into (10), we get:

$$\hat{d}_k^f = d_k^f + \Delta_k + \sqrt{\frac{P_n}{P_f}} \lambda + n_0, \quad (15)$$

where $\Delta_k = G(d_k^f) - d_k^f$ is the error vector caused by nonlinear distortion (Figure 2), which can be calculated using the operating point OBO, amplitude and phase distortion equations (4)–(7). n_0 is a Gaussian variable with a variance of $N_0/(2P_f T)$ and λ is the residual self-interference factor given by

$$\lambda = \left\{ \frac{\tau}{T} e^{j(2\pi f_c \tau + \phi)} - (1 + \eta) \frac{\tau + \Delta\tau}{T} \cdot e^{j[2\pi f_c(\tau + \Delta\tau) + \phi + \Delta\phi]} \right\} G(d_{k-1}^n) + \left\{ \frac{T - \tau}{T} \cdot e^{j(2\pi f_c \tau + \phi)} - (1 + \eta) \frac{T - \tau - \Delta\tau}{T} \cdot e^{j[2\pi f_c(\tau + \Delta\tau) + \phi + \Delta\phi]} \right\} G(d_k^n). \quad (16)$$

From (16), we know the residual self-interference is caused by two neighboring symbols: d_{k-1}^n and d_k^n .

The BER of M -QAM is different from the constellation area; see Figure 3. By using the classical method in [19], we get the BER:

$$P_e = \begin{cases} 1 - (1 - P_l)(1 - P_u - P_d), & d_k^f \in A_L, \\ 1 - (1 - P_l - P_r)(1 - P_d), & d_k^f \in A_D, \\ 1 - (1 - P_r)(1 - P_u - P_d), & d_k^f \in A_R, \\ 1 - (1 - P_l - P_r)(1 - P_u), & d_k^f \in A_U, \\ 1 - (1 - P_l)(1 - P_u), & d_k^f \in A_{LU}, \\ 1 - (1 - P_l)(1 - P_d), & d_k^f \in A_{LD}, \\ 1 - (1 - P_r)(1 - P_d), & d_k^f \in A_{RD}, \\ 1 - (1 - P_r)(1 - P_u), & d_k^f \in A_{RU}, \\ 1 - (1 - P_l - P_r)(1 - P_u - P_d), & d_k^f \in A_C, \end{cases} \quad (17)$$

where

$$P_l = Q \left\{ \sqrt{\frac{2E_b}{N_0 \log_2 M}} \left[\frac{D}{2} - \text{Re} \left(\Delta_k + \sqrt{P_n/P_f \lambda} \right) \right] \right\}, \quad (18)$$

$$P_r = Q \left\{ \sqrt{\frac{2E_b}{N_0 \log_2 M}} \left[\frac{D}{2} + \text{Re} \left(\Delta_k + \sqrt{P_n/P_f \lambda} \right) \right] \right\},$$

$$P_d = Q \left\{ \sqrt{\frac{2E_b}{N_0 \log_2 M}} \left[\frac{D}{2} - \text{Im} \left(\Delta_k + \sqrt{P_n/P_f \lambda} \right) \right] \right\},$$

and

$$P_u = Q \left\{ \sqrt{\frac{2E_b}{N_0 \log_2 M}} \left[\frac{D}{2} + \text{Im} \left(\Delta_k + \sqrt{P_n/P_f \lambda} \right) \right] \right\},$$

where $\text{Re}(\cdot)$ and $\text{Im}(\cdot)$ are for the real and imaginary parts and E_b is the energy per bit. The function Q is given by

$$Q(x) = \frac{1}{\sqrt{2\pi}} \int_x^\infty \exp(-t^2/2) dt.$$

D is the distance between constellation points, which can be calculated by

$$D = \frac{2\sqrt{M}}{\sqrt{\sum_{i=1}^{\sqrt{M}} \sum_{j=1}^{\sqrt{M}} [(2i-1-\sqrt{M})^2 + (2j-1-\sqrt{M})^2]}}. \quad (19)$$

The average BER of M -QAM full-duplex wireless communications can be written as

$$\bar{P}_e = \int_{-\infty}^{+\infty} P_e p(\lambda) d\lambda, \quad (20)$$

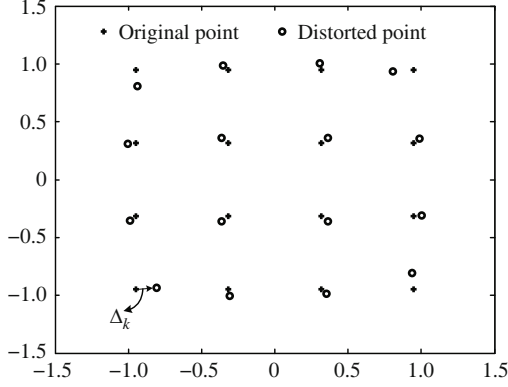


Figure 2 16-QAM constellation distorted by SSPA amplifier nonlinearity (OBO = 3 dB).

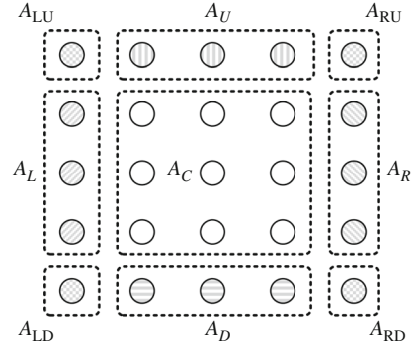


Figure 3 QAM constellation area.

where $p(\lambda)$ is the probability density function (PDF) of the residual self-interference factor λ .

To obtain the PDF of λ , we make an approximation to (16). In fact, the transmission delay $\Delta\tau$ is quite small, e.g., several nanoseconds or picoseconds, so $(\tau + \Delta\tau)/T \approx \tau/T$ and $(T - \tau + \Delta\tau)/T \approx (T - \tau)/T$, and the phase rotation $2\pi f_c \Delta\tau$ can be attributed to the phase estimation error $\Delta\phi$, so we omit $\Delta\tau$. Thus, λ can be rewritten as

$$\lambda \approx \alpha \left\{ e^{j\psi} - (1 + \eta)e^{j(\psi + \Delta\phi)} \right\} G(d_{k-1}^n) + (1 - \alpha) \left\{ e^{j\psi} - (1 + \eta)e^{j(\psi + \Delta\phi)} \right\} G(d_k^n), \quad (21)$$

where $\alpha = \tau/T$ is uniformly distributed in $[0, 1)$ and $\psi = 2\pi f_c \tau + \phi$ is uniformly distributed in $[0, 2\pi)$.

The characteristic function of λ is given by

$$\Phi(\omega) = E\{e^{j\omega\lambda}\} = \frac{1}{M^2} \sum_{x,y} \Phi_{x,y}(\omega), \quad (22)$$

where $\Phi_{x,y}(\omega)$ is the conditional characteristic function given by

$$\Phi_{x,y}(\omega) = \frac{1}{2\pi} \int_0^1 \int_{-\infty}^{\infty} \int_{-\infty}^{\infty} e^{j\omega\alpha[e^{j\psi} - (1+\eta)e^{j(\psi+\Delta\phi)}]G_x + j\omega(1-\alpha)[e^{j\psi} - (1+\eta)e^{j(\psi+\Delta\phi)}]G_y} p(\eta)p(\Delta\phi) d\eta d(\Delta\phi) d\alpha, \quad (23)$$

where $G_x, G_y \in \{G_1, G_2, \dots, G_M\}$ are the x th and y th M -QAM constellation points distorted by the amplifier nonlinearity. $p(\eta)$ and $p(\Delta\phi)$ are the PDFs of the interference estimation error η and $\Delta\phi$, which can be modeled as Gaussian variables with zero mean [20].

The PDF of the residual interference factor λ can be obtained from

$$p(\lambda) = \frac{1}{2\pi} \int_{-\infty}^{+\infty} \Phi(\omega) e^{-j\omega\lambda} d\omega. \quad (24)$$

The closed-form expression of (24) is difficult to obtain; however, it can be evaluated by numerical integration.

In this paper, a useful performance measure is the total degradation (TD) as a function of the amplifier OBO, which is given by [18]

$$\text{TD}_{\text{dB}} = \text{SNR}_{\text{dB}} - \text{SNR}'_{\text{dB}} + \text{OBO}, \quad (25)$$

where SNR_{dB} is the required signal-to-noise ratio in decibels for full-duplex wireless communications to obtain a fixed BER (e.g., 10^{-4}) for a given value of the OBO, and SNR'_{dB} is the required SNR to obtain the same BER in the absence of nonlinearity. The optimum operating point provides a good tradeoff between output power and degradation.

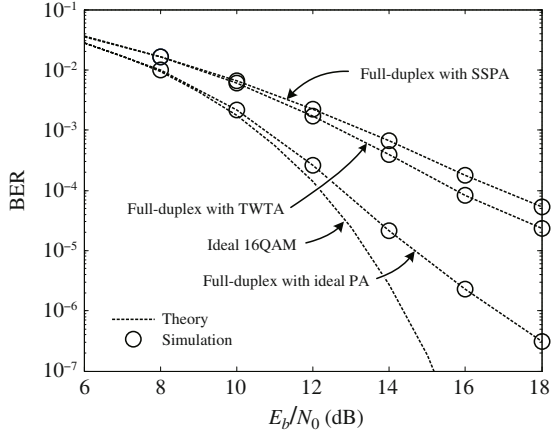


Figure 4 Average BER performance of 16-QAM full-duplex communications with nonlinear distortion when SIR = -40 dB and OBO = 3 dB.

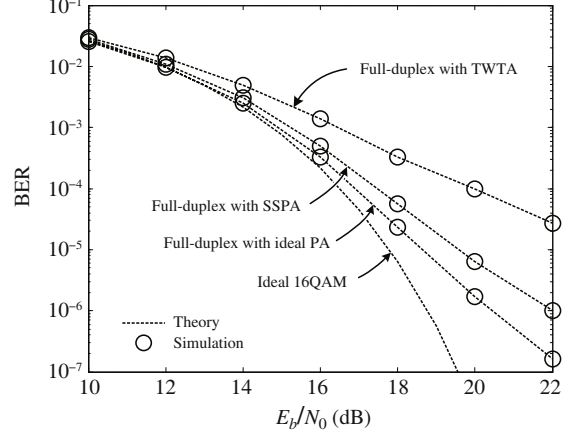


Figure 5 Average BER performance of 64-QAM full-duplex communications with nonlinear distortion when SIR = -33 dB and OBO = 7 dB.

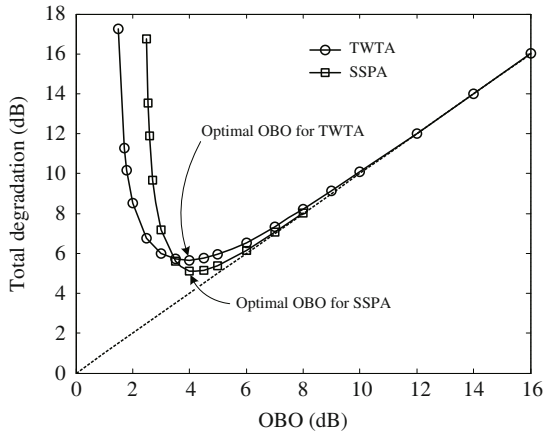


Figure 6 Total degradation of 16-QAM full-duplex communications when SIR = -40 dB.

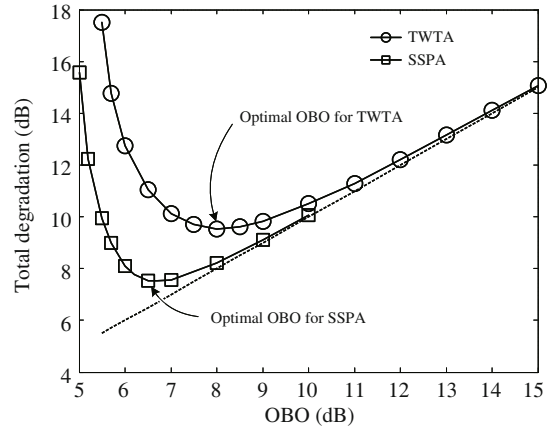


Figure 7 Total degradation of 64-QAM full-duplex communications when SIR = -33 dB.

4 Numerical results and discussions

In this section, numerical results are presented to evaluate the performance of a full-duplex system with nonlinear distortion. The system is set up as follows: the carrier frequency is 2 GHz and M -QAM is used with a symbol rate of 1.28 M/s. The relative amplitude error η and phase error $\Delta\phi$ are assumed to have Gaussian distributions [20] with standard deviations of 0.001 and 0.01° .

The theoretical results for \bar{P}_e are calculated using (20), and we can see the perfect agreement with the simulation results in Figures 4 and 5.

Figure 4 shows BER curves for 16-QAM when SIR = -40 dB and OBO = 3 dB. We can see performance degradation of 5 dB (respectively, 6.2 dB) caused by amplifier nonlinearity for TWTA (respectively, SSPA) at BER 10^{-4} , compared with an ideal amplifier.

Figure 5 shows BER curves for 64-QAM when SIR = -33 dB and OBO = 7 dB. We can see performance degradation of 0.6 dB (respectively, 3.1 dB) caused by amplifier nonlinearity for SSPA (respectively, TWTA) at BER 10^{-4} , compared with an ideal amplifier.

Figures 6 and 7 show TD versus OBO for 16- and 64-QAM full-duplex communications when SIR = -40 dB or -33 dB. The TD values were obtained with (20) and (25). It can be seen that TD firstly decreases with OBO, and finally increases with OBO. The BER performance was worse if OBO is too low, but it is a waste of amplifier ability if OBO is too large. It is possible to find the optimal OBO values for each system configuration considered from these figures.

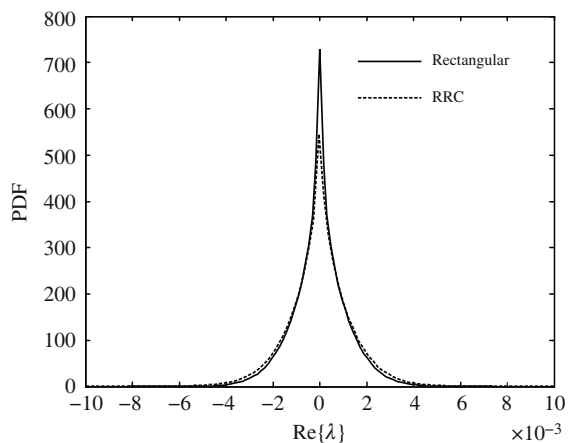


Figure 8 Probability density function of residual interference factor λ .

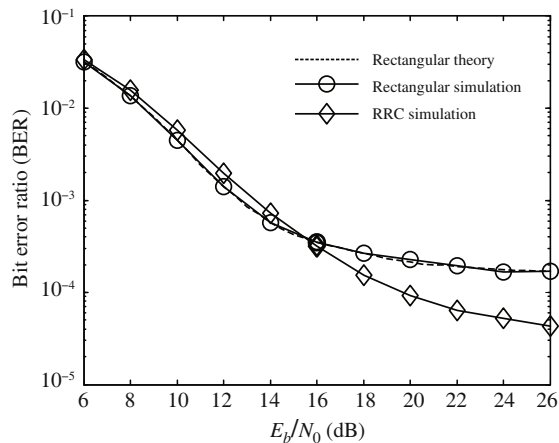


Figure 9 BER performance of 16-QAM full-duplex communications shaped by RRC or rectangular pulses with SIR = -30 dB and OBO = 6 dB for SSPA.

Figure 8 shows the PDF of residual interference factor $\text{Re}\{\lambda\}$ shaped by RRC and rectangular pulses. We can see that the two curves almost coincide and are different from a classic Gaussian PDF. The final influence of λ on BER can be evaluated by (20).

Figure 9 shows the performance of BER for 16-QAM full-duplex communications shaped by rectangular and RRC pulses. It can be seen that rectangular and RRC shaping curves decrease nearly parallel with E_b/N_0 (<15.5 dB). In particular, the rectangular shaping stayed about 0.6 dB ahead of RRC shaping at $\text{BER} = 10^{-3}$. However, when E_b/N_0 increases, both curves became flatter, and the RRC shaping had better BER performance.

5 Conclusion

In this paper, the effects of amplifier nonlinearities on full-duplex communications were evaluated. An expression for the BER was derived, which can be used to evaluate the performance degradation caused by amplifier nonlinearity and to find the best OBO value for amplifier configurations.

Acknowledgements This work was supported by National Natural Science Foundation of China (Grant Nos. 61531009, 61471108, U1035002/L05, 61001087, 61101034, 61271164, 61301154), National Major Projects (Grant Nos. 2014ZX03003001-002, 2012ZX03003010-003, 2011ZX03001-006-01), and National High-Tech R&D Program of China (863) (Grant No. 2014AA01A704).

Conflict of interest The authors declare that they have no conflict of interest.

References

- Ren P Y, Wang Y C, Du Q H. CAD-MAC: a channel-aggregation diversity based MAC protocol for spectrum and energy efficient cognitive ad hoc networks. *IEEE J Sel Areas Commun*, 2014, 32: 237–250
- Wu G, Ren P Y, Du Q H. Recall-based dynamic spectrum auction with the protection of primary users. *IEEE J Sel Areas Commun*, 2012, 30: 2070–2081
- Hong S, Brand J, Jung C, et al. Applications of self-interference cancellation in 5G and beyond. *IEEE Commun Mag*, 2014, 52: 114–121
- Zhang D D, Wang X, Zhang Z S. Key techniques research on full-duplex wireless communications (in Chinese). *Sci Sin Inform*, 2014, 44: 951–964
- Jain M, Choi J I, Kim T, et al. Practical, real-time, full duplex wireless. In: *Proceedings of 17th Annual International Conference on Mobile Computing and Networking*, Las Vegas, 2011. 301–312
- Choi J Y, Hur M S, Suh Y W, et al. Interference cancellation techniques for digital on-channel repeaters in T-DMB system. *IEEE Trans Broadcast*, 2011, 57: 46–56
- Lee Y J, Lee J B, Park S I, et al. Feedback cancellation for T-DMB repeaters based on frequency-domain channel estimation. *IEEE Trans Broadcast*, 2011, 57: 114–120

- 8 Duarte M, Sabharwal A. Full-duplex wireless communications using off-the-shelf radios: feasibility and first results. In: Proceedings of Asilomar Conference on Signals, Systems and Computers, Pacific Grove, 2010. 1558–1562
- 9 Duarte M, Sabharwal A, Aggarwal V, et al. Design and characterization of a full-duplex multi-antenna system for WiFi networks. *IEEE Trans Veh Technol*, 2014, 63: 1160–1177
- 10 White C R, Rebeiz G M. Single- and dual-polarized tunable slotting antennas. *IEEE Trans Antenn Propag*, 2009, 57: 19–26
- 11 Elsherbini A, Sarabandi K. Dual-polarized coupled sectorial loop antennas for UWB applications. *IEEE Antenn Wirel Propag Lett*, 2011, 10: 75–78
- 12 Guo Y X, Luk K M. Dual-polarized dielectric resonator antennas. *IEEE Trans Antenn Propag*, 2003, 51: 1120–1124
- 13 Korpi D, Riihonen T, Syrjala V, et al. Full-duplex transceiver system calculations: analysis of ADC and linearity challenges. *IEEE Trans Wirel Commun*, 2014, 13: 3821–3836
- 14 Bharadia D, McMilin E, Katti S. Full duplex radios. In: Proceedings of the ACM SIGCOMM 2013 Conference on SIGCOMM. New York: ACM, 2013. 375–386
- 15 Duarte M, Dick C, Sabharwal A. Experiment-driven characterization of full-duplex wireless systems. *IEEE Trans Wirel Commun*, 2012, 11: 4296–4307
- 16 Anttila L, Korpi D, Syrjala V, et al. Cancellation of power amplifier induced nonlinear self-interference in full-duplex transceivers. In: Proceedings of Asilomar Conference on Signals, Systems and Computers, Pacific Grove, 2013
- 17 Ahmed E, Eltawil A M, Sabharwal A. Rate gain region and design tradeoffs for full-duplex wireless communications. *IEEE Trans Wirel Commun*, 2013, 12: 3556–3565
- 18 Costa E, Pupolin S. *M-QAM-OFDM* system performance in the presence of a nonlinear amplifier and phase noise. *IEEE Trans Wirel Commun*, 2002, 50: 462–472
- 19 Proakis J. *Digital Communications*. 4th ed. New York: McGraw-Hill, 2001. 278–282
- 20 Su W M, Gu H, Ni J L, et al. Performance analysis of MVDR algorithm in the presence of amplitude and phase errors. *IEEE Antenn Wirel Propag Lett*, 2001, 49: 1875–1877